Subaperture Keystone Transform Matched Filtering Algorithm and Its Application for Air Moving Target Detection in an SBEWR System

Muyang Zhan, Chanjuan Zhao, Kun Qin, Penghui Huang, *Member, IEEE*, Ming Fang, and Chunlei Zhao

***Abstract*—Long-time coherent integration is an effective approach to improve detection performance for weak air moving targets (AMTs). The range position variation and azimuth Doppler variation will easily exceed range gate and Doppler resolution in a long observation time, resulting in severe performance degradation, especially for high maneuverability target. Besides, the high detection performance and low computational complexity ability are, most of times, the contradiction requirements by using the existing long-time coherent integration algorithms. To overcome above constraints, a novel subaperture keystone transform matched filtering (SAKTMF) method is developed in this article based on the conventional hybrid integration (HI) algorithm, which can realize coherent integration both within the subaperture and among subapertures, effectively improving the detection performance of a weak moving target. Furthermore, the proposed SAKTMF is applied for weak AMT detection in spaceborne early warning radar, which considers serious extended clutter, range migration, and Doppler migration problems simultaneously. Simulation experiments processing results show that the proposed method can provide improved detection performance compared with the conventional HI methods.**

***Index Terms*—Air moving target (AMT) detection, keystone transform (KT), long-time coherent integration, spaceborne early warning radar (SBEWR).**

I. Introduction

SPACEBORNE early warning radar (SBEWR) can provide many advantages in continuous global coverage, anti-stealth capabilities, and high safety features, which play a very important role in moving target surveillance [1], [2], [3]. With the rapid development of aviation and aerospace technology, threats from time-sensitive air moving targets (AMTs), such as stealth aircraft, cruise missiles, and near space hypersonic aerocraft, have become more frequent and difficult to be detected and tracked [4], [5]. In addition, due to the high-speed motion of the spaceborne platform, the observed moving targets may be easily submerged in the broadened ground/sea clutter background, making weak AMTs detection more challenging. To address this problem, post-Doppler space–time adaptive processing (STAP) techniques [6], such as extend factored approach [7], "filter-then-adapt" [8], and joint domain localized [9] have been proven to be effective tools to improve the output signal–clutter and noise ratios (SCNRs) of AMTs in an SBEWR system [10].

However, for an AMT with a low radar cross-section (RCS), the target energy is usually insufficient to exceed the expected detection threshold. Extending the observation time is an effective way to increase the target output signal-to-noise ratio (SNR); however, due to the high maneuverability of an AMT, undesirable range migration (RM) and Doppler frequency migration (DFM) will appear during the long dwell time [11], [12], resulting in a severe performance degradation in traditional moving target detection (MTD) method. To alleviate the influences of RM and DFM, many potential solutions [13], [14], [15], [16], [17], [18], [19], [20], [21], [22], [23], [24], [25], [26], [27], [28], [29], [30], [31], [32], [33], [34], [35], [36], [37], [38], [39], [40], [41] have been proposed in recent years, which can be mainly categorized into three types according to the integration modes: 1) noncoherent integration methods [13], [14]; 2) coherent integration methods [15], [16], [17], [18], [19], [20], [21], [22], [23], [24], [25], [26], [27], [28], [29], [30], [31], [32], [33], [34], [35], [36], [37], [38]; and 3) HI methods [39], [40], [41].

The most representative noncoherent integration method is Hough transform (HT) [13], [14], which integrates target energy along range history in range-compression domain by discarding phase information. However, the performance representation of HT method is limited by the poor noncoherent integration gain and this method may be more applicable for uniform motion target detection.

To improve detection performance and get the utmost out of the phase information, coherent integration methods are widely developed [15], [16], [17], [18], [19], [20], [21], [22], [23], [24],

Manuscript received 29 October 2022; revised 10 January 2023; accepted 30 January 2023. Date of publication 22 February 2023; date of current version 2 March 2023. This work was supported in part by the National Natural Science Foundation Program of China under Grant 62171272, Grant USCAST2021-15, and Grant SAST2019-071, and in part by the Shanghai Saliling Program under Grant 21YF1417400. This paper was presented in part at the China invention patent with title "An air moving target detection method and system for SBEWR based on subaperture processing" on April 2021. *(Corresponding author: Penghui Huang.)*

Muyang Zhan, Ming Fang, and Chunlei Zhao are with the Shanghai Aerospace Electronics Technology Institute, Shanghai 201108, China (e-mail: zhanmuyang1992@126.com; zj02065119@163.com; zhaochunlei24@hotmail.com).

Chanjuan Zhao and Kun Qin are with the Shanghai Aerospace Electronics Technology Institute, Shanghai 201108, China, and also with the National Laboratory of Radar Signal Processing, Xidian University, Xian 710071, China (e-mail: chanjuan1117@163.com; 35415505@qq.com).

Penghui Huang is with the School of Electronic Information and Electrical Engineering, Shanghai Jiao Tong University, Shanghai 200240, China (e-mail: huangpenghui@sjtu.edu.cn).

Digital Object Identifier 10.1109/JSTARS.2023.3245295

[25], [26], [27], [28], [29], [30], [31], [32], [33], [34], [35], [36], [37], which can be further subdivided into four categories, i.e., Radon-based methods [15], [16], [17], [18], [19], [20], [21], [22], [23], [24], keystone transform (KT)-based methods [25], [26], [27], [28], [29], matched filtering (MF)-based methods [30], [31], [32], and reduced-order (RO)-based methods [33], [34], [35], [36], [37]. The core idea of the RFT and GRFT is that the range and Doppler phase variations are compensated simultaneously by searching all possible target motion states. Followed by this main idea, many novel kernel functions are widely developed, including linear transform such as Radon-fractional Fourier transform [17], and nonlinear transform such as Radon-Lv's distribution [18], and others kernel function tools in [19], [20], [21], [22], [23], and [24]. In spite of the coherent integration gain can be obtained in these methods, the ergodic search operation in Radon-based methods will inevitably introduce unbearable computational burden. To alleviate the computation complexity, KT-based methods are proposed, such as KT [25], second-order KT [26], generalized KT, generalized dechirp process [27], and others modified KT [28], [29]. In these KT-based methods, certain order of RM can be first removed by KT or modified KT technique result in computation efficiency improvement, while may not deal with high-order maneuvering motions and high-speed target with Doppler ambiguous. Typical MF-based methods include KT matched filtering method [30], two-dimensional (2-D) matched filtering method [31], and series reversion method [32]. MF-based methods handle RM and DFM by implementing the time-domain or Doppler-domain MF processing, which can effectively accomplish target integration detection while still suffering from the heavy computational complexity since the searching operation is required. The RO-based methods [33], [34], [35], [36], [37] generally design a particular nonlinear kernel function to reduce the phase order of the radar returns and effectively alleviate the influence of the RM and DFM, leading to a rapid detection strategy. Typical RO-based methods including the adjacent cross-correlation function (ACCF) method [33], and range frequency reversals transform method [34]. Unfortunately, nonlinear operations may lead to unexpected performance losses.

To achieve a compromise between the target detection performance and real-time processing requirements, hybrid integration (HI) methods have been proposed in [38], [39], and [40], which joins subaperture coherent integration within subaperture and noncoherent processing among subapertures to realize target detection and track identification. In [38], the MTD and generalized Radon transform (GRT) are combined to reach this goal, which optimizes computational complexity with the sacrifice of the detection performance induced by incoherent integration among different slow-time subapertures.

Illuminated by the existing works [38], [39], [40], [41], [42], [43], in order to recover this part of performance loss and utilize the advantage of HI algorithm, in this article, a novel method, named subaperture keystone transform matched filtering (SAKTMF) is applied to improve the detection performance of AMTs in an SBEWR system. First, linear RM in whole-aperture is eliminated by performing the well-known KT. Then, the complete echo data are reasonably divided into multiple slow-time subapertures along the temporal dimension. Subsequently, a proper phase compensation function is constructed to eliminate the unwished phase difference among subapertures. Finally, another coherent integration operation is realized along different subapertures. By combining the advantages of HI and coherent integration, the proposed SAKTMF method can obtain entire coherent integration gains with relatively high computational complexity. After that, the SAKTMF is applied for weak AMT detection in SBEWR system as an alternative, which considers serious extended clutter, RM, and Doppler migration problems simultaneously. Performance analysis and simulation results show the superiority and effectiveness of the proposed SAKTMF method.

Relative to conventional methods, the proposed SAKTMF method has the following characteristics:

1) Compared with the GRFT method [16], the computation complexity is significantly degraded since searching dimension is reduced; in addition, the proposed SAKTMF method free from the BSSL influences, since the velocity ambiguity part can be compensated in advance [30].
2) Compared with the HI method in [38], the integration gain of the proposed SAKTMF method is improved benefited from the coherent integration gain among different subapertures.
3) Compared with nonlinear kernel function based methods in [18], [19], [20], [21], [22], [23], and [24] and [33], [34], [35], [36], and [37], the proposed method is immune to performance loss induced by nonlinear operation, resulting in applicable in low SNR environment.
4) Compared with the methods in [13] and [14], and [17], [26], [27], [28], [28], [30], [31], [32], [33], [34], [35], [36], [37], and [38], and modified HI methods [41], [42], [43] which is designed for particular motion model, the proposed method can be applied for target with arbitrary motion order. In addition, clutter influence for SBEWR is considered in this article.

The remainder of this article is outlined as follows. Section II presents the conventional signal model. Section III introduces the proposed SAKTMF method in details. Section IV describes the application of proposed SAKTMF in an SBEWR for AMT detection. In Section V, numerical simulations of MTD and performance comparisons are demonstrated to validate the effectiveness of the proposed methods. In Section VI, some discussions for the proposed method are introduced. Some conclusions are drawn in Section VII to close this article.

II. Conventional Signal Model

Typically, a linear frequency modulated (LFM) waveform is adopted as the transmission signal to ensure adequate time-bandwidth product, which can be expressed as

$$s(t_r) = \text{rect}(t_r/T_p)\exp\left[j2\pi\left(f_c t_r + \gamma t_r^2/2\right)\right] \quad (1)$$

where $\text{rect}(\cdot)$ denotes the rectangle window function, symbols t_r, T_p, f_c, and γ being the range fast-time variable, the pulse duration time, the carrier frequency, and the LFM chirp rate, respectively.

Suppose that there is an uncooperative moving radar to be illuminated over the entire radar observation period, different from the methods in [17], [18], [19], [20], [21], [22], [23], [24], [25], [26], [27], [28], [29], [30], [31], [32], [33], [34], [35], [36], and [37], here the instantaneous slant-range between radar and moving target is modeled by the arbitrary *K*-order polynomial, i.e.

$$R(t_m) = \sum_{k=0}^{K} \frac{x_k}{k!} t_m^k, t_m \in \left[-\frac{T_a}{2}, \frac{T_a}{2}\right] \tag{2}$$

where t_m is the azimuth slow-time variable, x_k is the motion parameters of *k* order, *K* denotes the maximum polynomial order, and T_a is the dwell time.

After range pulse compression (PC) and demodulation operation, the received radar echoes signal in the range-frequency and slow-time domain can be noted as [17]

$$\begin{aligned} Ss(f_r, t_m) &= \sigma \text{rect}\left[\frac{f_r}{B}\right] \text{rect}\left[\frac{t_m}{T_a}\right] \\ &\times \exp\left[-j\frac{4\pi(f_r + f_c)}{c} R(t_m)\right] \end{aligned} \tag{3}$$

where f_r is the range frequency variable, σ is the complex amplitude, B is the range bandwidth, and c is the speed of light. After performing the range inverse fast Fourier transform (IFFT), the received echoes signal can be further described as

$$\begin{aligned} ss(t_r, t_m) &= A\text{rect}\left[\frac{t_m}{T_a}\right] \text{sinc}\left\{B\left[t_r - 2R(t_m)/c\right]\right\} \\ &\times \exp\left[-j\frac{4\pi}{\lambda} R(t_m)\right] \end{aligned} \tag{4}$$

where sinc$(\cdot)$ denotes the sin*c* function and λ is the wavelength of the emission signal. From (4), it can be easily observed that the time-varying slant-range $R(t_m)$ will lead to the peak position variation in range direction and Doppler variation in the azimuth dimension. For a high-maneuvering target, the RM and DFM will occur when the following conditions are satisfied:

$$\text{RM} = \sum_{k=1}^{K} \frac{x_k}{k!} T_a^k > \frac{c}{2B} \tag{5}$$

$$\text{DFM} = \frac{2}{\lambda} \sum_{k=2}^{K} \frac{x_k}{(k-1)!} T_a^{k-1} > \frac{1}{T_a} \tag{6}$$

where RM and DFM are the maximum variations in the range and Doppler dimensions, respectively. In order to realize the improvement of detection performance for weak targets by extending the observation time, the above RM and DFM should be effectively processed.

III. Proposed SAKTMF Method

In this section, the HI algorithm [38] is first introduced concisely. After that, following the main idea of the HI algorithm, the SAKTMF method is established in details based on two steps coherent integration strategy.

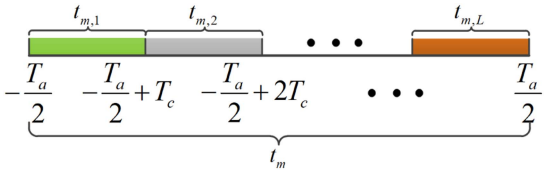

Fig. 1. Diagram of azimuth time division.

A. Review of Conventional HI Detection Algorithm

Suppose that the whole echo data in (4) is uniformly divided into *L* subblocks, each of subintervals contains N_c sample numbers and subinterval dwell time is $T_c = T_a/L$. Then, the echo signal in (4) can be rewritten as [38], [39], [40], [41], [42], and [43]

$$ss(t_r, t_m) = \sum_{l=1}^{L} ss_l(t_r, t_{m,l}) \tag{7}$$

with the *l*th subaperture echo expression

$$\begin{aligned} ss_l(t_r, t_{m,l}) &= A\text{rect}\left[\frac{t_{m,l}}{T_a}\right] \text{sinc}\left\{B\left[t_r - 2R(t_{m,l})/c\right]\right\} \\ &\times \exp\left[-j\frac{4\pi}{\lambda} R(t_{m,l})\right] \end{aligned} \tag{8}$$

where $t_{m,l} \in [-T_a/2 + (l-1)T_c, -T_a/2 + lT_c), (l = 1, 2, \ldots, L)$ is the segmented azimuth time variable, whose partition diagram is displayed in Fig. 1.

The principle of azimuth subaperture division is based on the constraint that RM and DFM do not occur within the subaperture, i.e.,

$$\Delta\text{RM} = \sum_{k=1}^{K} \frac{x_k}{k!} T_c^k \le \frac{c}{2B} \tag{9}$$

$$\Delta\text{DFM} = \frac{2}{\lambda} \sum_{k=2}^{K} \frac{x_k}{(k-1)!} T_c^{k-1} \le \frac{1}{T_c} \tag{10}$$

where ΔRM and ΔDFM are the maximum variations along the range and Doppler direction in a subaperture, respectively. Under this constraint, the target can be preliminarily integrated by performing the azimuth fast Fourier transform (FFT) in each subaperture, one has

$$sS_l(t_r, f_m) = \text{FFT}_{t_m}\left[ss_l(t_r, t_{m,l})\right] \tag{11}$$

where $\text{FFT}_{t_m}[\cdot]$ denotes performing FFT operation with respect to t_m, and f_m denotes Doppler frequency.

Finally, the incoherent integration among subapertures is carried out by using GRT [38], which can be noted as

$$\text{HI}\{\boldsymbol{\alpha}\} = \sum_{l=1}^{L} \left| sS_l\left(\frac{2}{c} r(\boldsymbol{\alpha}, lT_c), f(\boldsymbol{\alpha}, lT_c)\right)\right| \tag{12}$$

where $\boldsymbol{\alpha}$ is the searching parametric space vector, $r(\boldsymbol{\alpha}, lT_c)$ and $f(\boldsymbol{\alpha}, lT_c)$ denote the range and Doppler position corresponding to the subaperture index l and searching motion parameter space $\boldsymbol{\alpha}$, respectively.

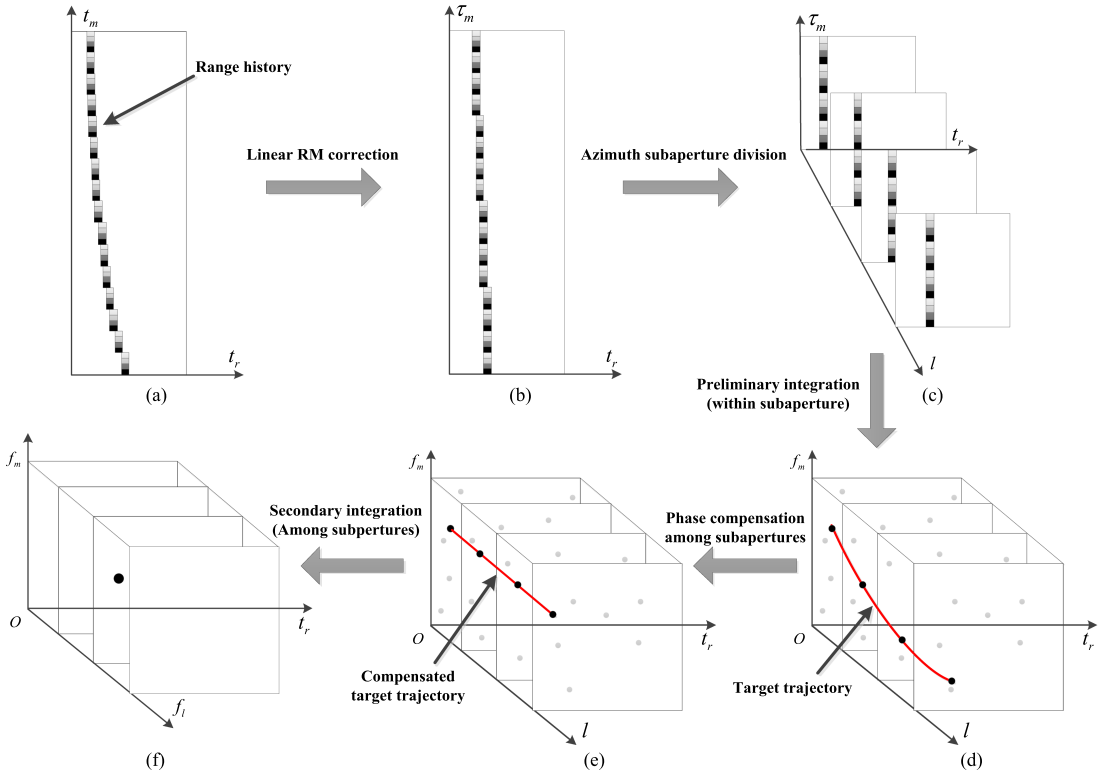

Fig. 2. Flow chart of the proposed SAKTMF method. (a) Range profile in the range-compressed domain. (b) Range profile after linear RM correction by KT. (c) Azimuth subaperture division. (d) Preliminary integration within subaperture by MTD. (e) Phase compensation among subapertures. (f) Secondary integration among different subapertures by subaperture FFT.

B. SAKTMF Algorithm

Conventional HI method in [38] only considers the focused positions change among the subapertures, while discarding the phase differences for different subapertures. Motivated by the methods in [38], [39], [40], [41], [42], and [43], a novel SAKTMF method is developed based on the phase relationship derivation among subapertures, whose main steps are listed as follows: 1) linear RM correction by the KT; 2) azimuth subaperture division and preliminary integration within subaperture; and 3) phase compensation and secondary coherent integration among subapertures. Fig. 2 shows the flow chart of the proposed SAKTMF method.

1) Linear Range Migration Correction: The KT with $(f_r + f_c)t_m = f_c\tau_m$ is first performed on (3) to accomplish linear RM correction [25].Then, one can obtain

$$Ss\left(f_r,\tau_m\right) = \sigma \mathrm{rect}\left[\frac{f_r}{B}\right]\mathrm{rect}\left[\frac{f_c}{f_r+f_c}\frac{\tau_m}{T_a}\right] \times \exp\left[-j\frac{4\pi\left(f_r+f_c\right)}{c}\sum_{k=0}^{K}\frac{x_k}{k!}\left(\frac{f_c}{f_r+f_c}\right)^k\tau_m^k\right] \tag{13}$$

where τ_m is the new azimuth time variable.

According to the Taylor series expansion around the range frequency variable f_r, we have

$$\left(\frac{f_c}{f_r+f_c}\right)^k \approx 1 - k\frac{f_r}{f_c}. \tag{14}$$

Substituting (14) in (13), one can obtain

$$\begin{aligned} Ss\left(f_r,\tau_m\right) \approx{}& \sigma \mathrm{rect}\left[\frac{f_r}{B}\right]\mathrm{rect}\left[\frac{f_c}{f_r+f_c}\frac{\tau_m}{T_a}\right] \\ &\times \exp\left[-j\frac{4\pi\left(f_r+f_c\right)}{c}x_0\right] \\ &\times \exp\left(-j\frac{4\pi}{\lambda}\sum_{k=1}^{K}\frac{x_k}{k!}\tau_m^k\right) \\ &\times \exp\left[j\frac{4\pi f_r}{c}\sum_{k=1}^{K}\left(k-1\right)\frac{x_k}{k!}\tau_m^k\right]. \end{aligned} \tag{15}$$

Clearly, the linear coupling relationship between f_r and first-order term of τ_m is effectively eliminated.

2) Azimuth Subaperture Division: To avoid the high-order RM and DFM in each subinterval, the azimuth subaperture division technique is subsequently adopted. And the echo signal in (15) can be rewritten as the following summation form [38],

[39], [40], [41], [42], [43]

$$Ss\left(f_r,\tau_m\right)=\sum_{l=1}^{L}Ss_l\left(f_r,\tau_{m,l}\right) \tag{16}$$

with lth subaperture echo given by

$$\begin{aligned}Ss_l\left(f_r,\tau_{m,l}\right)=&\sigma\text{rect}\left[\frac{f_r}{B}\right]\text{rect}\left[\frac{f_c}{f_r+f_c}\frac{\tau_{m,l}}{T_c}\right]\\&\times\exp\left[-j\frac{4\pi\left(f_r+f_c\right)}{c}x_0\right]\\&\times\exp\left(-j\frac{4\pi}{\lambda}\sum_{k=1}^{K}\frac{x_k}{k!}\tau_{m,l}^{k}\right)\\&\times\exp\left[j\frac{4\pi f_r}{c}\sum_{k=1}^{K}\left(k-1\right)\frac{x_k}{k!}\tau_{m,l}^{k}\right]\end{aligned} \tag{17}$$

where $\tau_{m,l}\in[-T_a/2+(l-1)T_c,-T_a/2+lT_c),\ (l=1,2,\ldots,N_c)$ is the segmented slow-time variable after performing the KT.

Considering that $\tau_{m,l}=\tau_{m,1}+l\cdot T_c$, the relationship between the lth subaperture and reference subaperture (first subaperture) echo can be expressed as

$$Ss_l\left(f_r,\tau_{m,l}\right)=Ss_1\left(f_r,\tau_{m,1}\right)\times\Delta\varphi_l\left(f_r,\tau_{m,1}\right) \tag{18}$$

with the phase difference given by

$$\begin{aligned}&\Delta\varphi_l\left(f_r,\tau_{m,1}\right)\\&=\exp\left[-j\frac{4\pi}{\lambda}\sum_{k=1}^{K}\left(\sum_{r=0}^{k-1}\frac{x_k}{k!}C_k^r(lT_c)^{k-r}\tau_{m,1}^{r}\right)\right]\\&\quad\times\exp\left[j\frac{4\pi f_r}{c}\sum_{k=1}^{K}\left(\sum_{r=0}^{k-1}\frac{\left(k-1\right)x_k}{k!}C_k^r(lT_c)^{k-r}\tau_{m,1}^{r}\right)\right].\end{aligned} \tag{19}$$

The phase relationship in (19) indicates the phase difference among subapertures after KT and subaperture division operations, which relates to the target motion parameters and subaperture index. Within the subaperture, the RM and DFM caused by the higher order phase can be ignored and the preliminary coherent integrated result after the range IFFT and azimuth FFT of (18) can be expressed as

$$\begin{aligned}&sS_l\left(t_r,f_m;l\right)\\&\approx A'\text{sinc}\left\{B\left[t_r-2\left(x_0-\sum_{k=1}^{K}\left(k-1\right)\frac{x_k}{k!}(lT_c)^{k}\right)\Big/c\right]\right\}\\&\quad\times\text{sinc}\left\{T_c\left[f_m+\frac{2}{\lambda}\sum_{k=1}^{K}\left(\frac{x_k}{(k-1)!}(lT_c)^{k-1}\right)\right]\right\}\\&\quad\times\exp\left[-j\frac{4\pi}{\lambda}\sum_{k=0}^{K}\frac{x_k}{k!}(lT_c)^{k}\right]\end{aligned} \tag{20}$$

where A' is integrated amplitude. It can be clearly observed that target peak position varies with different subaperture, which is determined by the high-order motion parameters of the target and the subaperture index.

3) Subaperture Coherent Integration: Based on the phase relationship in (18), construct the following phase compensation function to remove the phase variation among subapertures caused by the high-order motion parameters, i.e.

$$\begin{aligned}&H_{l,\text{comp}}\left(f_r,\tau_{m,1};\tilde{\boldsymbol{x}}\right)\\&=\exp\left[j\frac{4\pi}{\lambda}\sum_{k=1}^{K}\left(\sum_{r=0}^{k-1}\frac{\tilde{x}_k}{k!}C_k^r(lT_c)^{k-r}\tau_{m,1}^{r}\right)\right]\\&\quad\times\exp\left[-j\frac{4\pi f_r}{c}\sum_{k=1}^{K}\left(\sum_{r=0}^{k-1}\frac{\left(k-1\right)\tilde{x}_k}{k!}C_k^r(lT_c)^{k-r}\tau_{m,1}^{r}\right)\right]\end{aligned} \tag{21}$$

where $\tilde{x}_k(k=2,\cdots,K)$ denotes searching motion parameters, and corresponding searching motion parameters vector is denoted by $\tilde{\boldsymbol{x}}$.

Suppose that searching motion parameters match the true value well, i.e., $\tilde{x}_k=x_k(k=2,\cdots,K)$, the lth subaperture echo signal after multiplying with the phase compensation function in (21) can be expressed as

$$Ss_{l,\text{comp}}\left(f_r,\tau_{m,l}\right)=Ss_1\left(f_r,\tau_{m,l}\right)\exp\left[-j\frac{4\pi}{\lambda}x_1lT_c\right]. \tag{22}$$

After that, followed by the preliminary coherent integration within subaperture by taking range IFFT and azimuth FFT on (22), secondary coherent integration can be implemented by subaperture FFT, whose expression is shown as follows:

$$\begin{aligned}&sS'_{t,l}\left(t_r,f_m,f_l\right)\\&\approx LA'\cdot\text{sinc}\left[B\left(t_r-\frac{2x_0}{c}\right)\right]\text{sinc}\left[T_c\left(f_m+\frac{2}{\lambda}x_1\right)\right]\\&\quad\times\text{sinc}\left[N_c\left(f_l+\frac{2}{\lambda}x_1T_c\right)\right]\exp\left[-j\frac{4\pi}{\lambda}\left(x_0+x_1lT_c\right)\right]\end{aligned} \tag{23}$$

where f_l is defined as the subaperture frequency variable with respect to l. From (23), it can be observed that the target will be completely focused at the corresponding range gate, Doppler gate, and subaperture frequency gate. In addition, target energy is coherently and fully integrated, and the proposed SAKTMF can be concluded as

$$\begin{aligned}\text{SAKTMF}\left(t_r,f_m;\tilde{\boldsymbol{x}}\right)=\text{FFT}_l\{\text{FFT}_{\tau_m}\{\text{IFFT}_{f_r}[&S_l\left(f_r,\tau_{m,l}\right)\\&\times H_{l,\text{comp}}\left(f_r,\tau_{m,1};\tilde{\boldsymbol{x}}\right)]\}\}\end{aligned} \tag{24}$$

where $\text{IFFT}_{f_r}[\cdot]$, $\text{FFT}_{\tau_m}[\cdot]$, and $\text{FFT}_l[\cdot]$ represent performing IFFT along the range frequency, and FFT along the azimuth and subaperture direction, respectively. In the meantime, the motion parameters can be, respectively, estimated as

$$\hat{x}_1=-\frac{2}{\lambda}\left[\arg\max_{\hat{f}_m}\left\{\text{SAKTMF}\left(t_r,f_m;\tilde{\boldsymbol{x}}\right)\right\}\right] \tag{25}$$

$$\hat{\boldsymbol{x}}=\arg\max_{\tilde{\boldsymbol{x}}}\left\{\text{SAKTMF}\left(t_r,f_m;\tilde{\boldsymbol{x}}\right)\right\}. \tag{26}$$

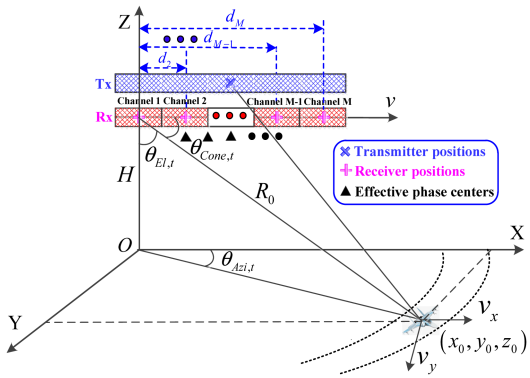

Fig. 3. Geometry relationship between the SBEWR platform and an AMT.

IV. Applications for AMT Detection in an SBEWR System

In this section, the SAKTMF method is applied in an SBEWR system, so as to improve the detection performance for a weak AMT, where the second-order motion model is considered instead of arbitrary order in this scenario.

A. Signal Model for an SBEWR System

The 3-D geometry between an SBEWR platform with a height of H and an AMT located at (x_0, y_0, z_0) is shown in Fig. 3. In an SBEWR system, the whole antenna aperture is usually applied to transmit the radar signal to enhance the output energy of a weak AMT. The azimuth receiving antenna is uniformly divided into M subarrays in order to provide enough spatial freedom. The distance of the mth receive channel with respect to the reference (first) channel is $d_m = m \cdot d, m = 0, 1, \ldots, M-1$, where d is the physical distance between two adjacent channels. v is the platform velocity, and v_x and v_y denote the target along- and cross-track velocities, respectively. The angles $\theta_{\text{El},t}$, $\theta_{\text{Azi},t}$,and $\theta_{\text{Cone},t}$ are the elevation angle, azimuth angle, and cone angle of this AMT, respectively.

According to Fig. 3, the equivalent self-transmitting and self-receiving slant range between an AMT and the mth receive channel can be calculated as

$$R_{t,m}(t_a) = \sqrt{\begin{matrix}[(v - v_x)\, t_a + (D + d_m)/2 - x_0]^2 \\ +(y_0 + v_y t_a)^2 + (H - z_0)^2\end{matrix}} \tag{27}$$

where t_a is the azimuth slow-time variable and $D = M \cdot d$ is the whole azimuth size of the transmitted antenna. According to second-order Taylor expansion and by performing a chirp deramp by using the platform parameters [25], one can obtain

$$R_{0t,m}(t_a) \approx R_0 - \frac{D + d_m}{2} \cos\theta_{Azi,t} \sin\theta_{El,t} + v_e t_a + \frac{1}{2}\alpha_e t_a^2 \tag{28}$$

where $R_0 = \sqrt{x_0^2 + y_0^2 + (H - z_0)^2}$ is the nearest slant range, $v_e = v_y \sin\theta_{\text{Azi},t} \sin\theta_{\text{El},t} - v_{rx} \cos\theta_{\text{Azi},t} \sin\theta_{\text{El},t}$ is the equivalent radial velocity with the relative platform velocity $v_{rx} = v - v_x$, and $\alpha_e = [-2vv_x + v_x^2 - (v_{rx}\cos\theta_{\text{Azi},t} \sin\theta_{\text{El},t} + v_y \sin\theta_{\text{Azi},t} \sin\theta_{\text{El},t})^2]/R_0$ is the residual second-order coefficient related to the target unknown motion parameters.

After PC, the received baseband echo signal of the mth received channel can be denoted as [10]

$$ss_{t,m}(t_r, t_a) = A_t \text{rect}\left(\frac{t_a}{T_a}\right) \text{sinc}\left[B\left(t_r - \frac{2R_{0t,m}(t_a)}{c}\right)\right] \times \exp\left[-j\frac{4\pi}{\lambda} R_{0t,m}(t_a)\right] \tag{29}$$

where $A_t = P_t \tau B G_T(\theta_{\text{Azi},t}, \theta_{\text{El},t}) G_{R\_\text{Sub}}(\theta_{\text{Azi},t}, \theta_{\text{El},t}) \lambda^2 \sigma / (4\pi)^3 R_0^4 L_s$ is the target echo amplitude calculated by the radar equation; the symbols P_t, τ, B, $G_T(\theta_{\text{Azi},t}, \theta_{\text{El},t})$, $G_{R\_\text{Sub}}(\theta_{\text{Azi},t}, \theta_{\text{El},t})$, λ, L_s, and σ are the peak power, pulsewidth, signal bandwidth, full aperture gain of the transmitting antenna, subchannel gain of the receiving antenna, wavelength, system loss, and target RCS, respectively.

In this article, we consider enhancing the target output SCNR by prolonging the observation time; as a consequence, RM and DFM, in virtue of target motion, should be taken into account, where the range curvature in (29) is ignored since it is usually less than a range resolution cell in an SBEWR [1].

B. Application of Proposed SAKTMF Method

In order to improve the detection performance for a weak AMT, we apply the proposed SAKTMF method in SBEWR system with some minor revisions and the processing procedures of the proposed scheme are shown in Fig. 4. In the following derivations, echo signal begins with completed preprocessing steps, including clutter compensation and linear RM correction by KT, which can be expressed as

$$ss_{t,m}(t_r, \tau_a) \approx A_t \text{rect}\left(\frac{\tau_a}{T_a}\right) \text{sinc}\left[B\left(t_r - \frac{2R_0}{c}\right)\right] \times \exp\left[-j\frac{4\pi}{\lambda}\left(R_0 - \frac{(D + d_m)}{2}\cos\theta_{\text{Azi},t}\sin\theta_{\text{El},t} + v_e\tau_a + \frac{1}{2}\alpha_e\tau_a^2\right)\right] \tag{30}$$

where τ_a is the azimuth time variable after performing KT.

1) Slow-Time Subaperture Division: In recent years, many studies [15], [16], [17], [18], [19], [20], [21], [22], [23], [24], [25], [26], [27], [28], [29], [30], [31], [32], [33], [34], [35], [36], [37] have addressed the problem of DFM based on motion parameter searching and accomplished target refocusing under the hypothesis that potential moving targets have been detected. However, the existence of an AMT in SBEWR echoes is unknown in advance; in addition, under the condition of fixed revisit time, the real-time requirement of the SBEWR is very urgent to realize the wide surveillance of the terrain of interest. Therefore, the above parameter-estimation-based methods may not be suitable for AMT detection in an SBEWR system.

To address this contradiction between the presence of a potential AMT and the real-time processing requirement, the influence of DFM is alleviated by using slow-time subaperture division

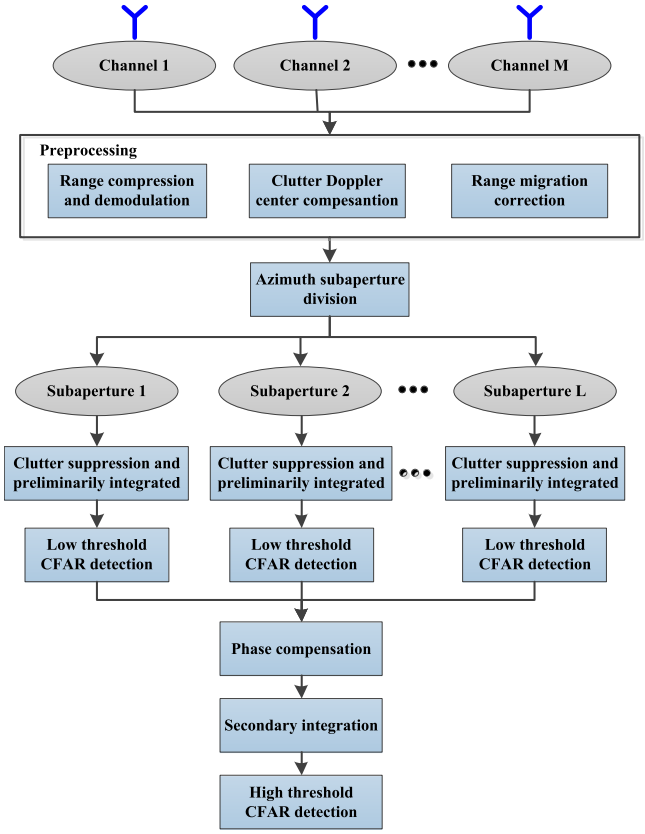

Fig. 4. Processing procedures of the proposed method for AMT in SBEWR.

technique. Suppose that the whole echo signal is divided into L subintervals, which can be rewritten as

$$ss_{t,m}\left(t_r,\tau_a\right)=\sum_{l=1}^{L}ss_{t,m,l}\left(t_r,\tau_{a,l}\right) \tag{31}$$

where $\tau_{a,l}$ is the segmented temporal variable. In each subaperture, DFM can be ignored and the AMT signal can be initially focused by performing the azimuth FFT, i.e.

$$\begin{aligned}&sS_{t,m,l}\left(t_r,f_m\right)\\&=A_t'\mathrm{sinc}\left[B\left(t_r-\frac{2R_0}{c}\right)\right]\mathrm{sinc}\left\{T_c\left[f_m+\frac{2}{\lambda}\left(v_e+\alpha_e lT_c\right)\right]\right\}\\&\quad\times\exp\left[j\frac{2\pi\left(D+d_m\right)}{\lambda}\cos\theta_{\mathrm{Azi},t}\sin\theta_{\mathrm{El},t}\right]\\&\quad\times\exp\left[-j\frac{4\pi}{\lambda}\left(R_0+v_e lT_c+\frac{1}{2}\alpha_e l^2T_c^2\right)\right]\end{aligned} \tag{32}$$

where $A_t'=P_{\mathrm{av}}T_cBG_T(\theta_{\mathrm{Azi},t},\theta_{\mathrm{El},t})G_{R\_\mathrm{Sub}}(\theta_{\mathrm{Azi},t},\theta_{\mathrm{El},t})\lambda^2\sigma/(4\pi)^3R_0^4L_s$ is the signal amplitude and P_{av} is the radar average power.

2) Clutter Rejection: By using the multichannel configuration, for the lth subaperture and mth azimuth channel, the echo data of $x_{m,l}(t_{r0},f_{a0})$ in t_r-f_a domain can be arranged into a vector $\boldsymbol{X}_l(t_{r0},f_{a0})=[x_{1,l}(t_{r0},f_{a0}),\ldots,x_{M,l}(t_{r0},f_{a0})]^T$, which is formulated as

$$\begin{aligned}H_0:\boldsymbol{X}_l\left(t_{r0},f_{a0}\right)&=\boldsymbol{sS_{c},}_l\left(t_{r0},f_{a0}\right)+\boldsymbol{n}_l\left(t_{r0},f_{a0}\right)\\H_1:\boldsymbol{X}_l\left(t_{r0},f_{a0}\right)&=\boldsymbol{sS_{t},}_l\left(t_{r0},f_{a0}\right)+\boldsymbol{sS_{c},}_l\left(t_{r0},f_{a0}\right)\\&\quad+\boldsymbol{n}_l\left(t_{r0},f_{a0}\right)\end{aligned} \tag{33}$$

where hypotheses H_0 and H_1 represent the detection cell without an AMT and the detection cell with an AMT, respectively. $\boldsymbol{sS}_{t,l}(t_{r0},f_{a0})$, $\boldsymbol{sS}_{c,l}(t_{r0},f_{a0})$, and $\boldsymbol{n}_l(t_{r0},f_{a0})$ denote the multichannel signal components of an AMT, clutter, and Gaussian white noise, respectively. According to (32), the multichannel AMT signal is given by

$$\boldsymbol{sS_{t},}_l\left(t_{r0},f_{a0}\right)=\left[sS_{t,1,l}\left(t_{r0},f_{a0}\right),\ldots,sS_{t,M,l}\left(t_{r0},f_{a0}\right)\right]^T. \tag{34}$$

In addition, the multichannel clutter signal can also be obtained by using a similar derivation with the scatterer velocity setting as zeros [10]. According to (34), the post-Doppler STAP is implemented in the lth subaperture to realize clutter suppression, which can be expressed as

$$\begin{cases}\min\limits_{\boldsymbol{W}} & \boldsymbol{W}_l^H\hat{\boldsymbol{R}}_{\mathrm{sub},l}\boldsymbol{W}_l\\ \text{s.t.} & \boldsymbol{W}_l^H\boldsymbol{S}=1\end{cases} \tag{35}$$

where $\boldsymbol{S}$ is the spatial-time steering vector of an AMT, $\boldsymbol{W}_l$ is the clutter rejection weight vector of the lth subaperture, and $\hat{\boldsymbol{R}}_{\mathrm{sub},l}$ is the covariance matrix estimated from the adjacent I range cells according to $\hat{\boldsymbol{R}}_{\mathrm{sub},l}=\sum_{i=1}^{I}\boldsymbol{X}_l(t_{r0,i},f_{a0})\boldsymbol{X}_l(t_{r0,i},f_{a0})^H/I$. $t_{r0,i}$ $(i=1,\cdots,I)$ denotes the range time with respect to the selected range samples.

Finally, the adaptive filter output is

$$Y_l\left(t_{r0},f_{a0}\right)=\boldsymbol{W}_{\mathrm{opt},l}^H\boldsymbol{X}_l\left(t_{r0},f_{a0}\right) \tag{36}$$

where the optimal weight vector $\boldsymbol{W}_{\mathrm{opt},l}=\mu_l\hat{\boldsymbol{R}}_{\mathrm{sub},l}^{-1}\boldsymbol{S}$, and the normalized scalar $\mu_l=\boldsymbol{S}^H\hat{\boldsymbol{R}}_{\mathrm{sub},l}^{-1}\boldsymbol{S}$ is the normalized scalar.

After that, the target energy is coherently synthesized in the spatial domain but is still dispersed among the temporal subapertures. Thus, initial CFAR detection with low threshold V_{LT} is performed on the reference subaperture to extract the range-Doppler positions of the potential targets, which can be described as

$$T_{\mathrm{LowThre}}=Y_l\left(t_{r0},f_{a0}\right)\underset{H_0}{\overset{H_1}{\gtrless}}V_{\mathrm{LT}}. \tag{37}$$

3) Subaperture Coherent Processing: Assume that $ss'_{t,l}(t_r,\tau_{a,l})$ denotes the target echo signal after performing the azimuth IFFT on (36), the relationship among subapertures can be noted as

$$ss'_{t,l}\left(t_r,\tau_{a,l}\right)=ss'_{t,1}\left(t_r,\tau_{a,1}\right)\times\Delta\varphi_l\left(\tau_{a,1}\right) \tag{38}$$

with the phase difference given by

$$\Delta\varphi_l\left(\tau_{a,1}\right)=-j\frac{4\pi}{\lambda}\left(v_e lT_c+\frac{1}{2}\alpha_e l^2T_c^2+\alpha_e lT_c\tau_{a,1}\right). \tag{39}$$

Different from (19), the phase term in (39) ignores the RM terms since the RM has been removed by KT in a narrow-band

TABLE I
RADAR SYSTEM PARAMETERS

Parameter	Value	Parameter	Value
Carrier frequency	3 GHz	Range pulse number	208
LFM Bandwidth	20 MHz	Azimuth pulse number	3000
Sample frequency	30 MHz	Subaperture number	50
Pulse duration	2 μs	Subaperture pulse number	60
Pulse Repetition Frequency	1500 Hz	Coherent processing time	2 s

SBEWR system. Thus, the corresponding phase compensation function degrades into the following 1-D form, i.e.

$$H_{l,\text{comp}}\left(\tau_{a,1};\alpha_e\right)=\exp\left[j\frac{4\pi}{\lambda}\left(\alpha_e l T_c\tau_{a,1}+\frac{1}{2}\alpha_e l^2 T_c^2\right)\right]. \tag{40}$$

It should be noted that the computational cost in this step is low since only a 1-D search is involved; additionally, piecewise processing effectively reduces the data length in each search, resulting in higher computational efficiency.

When the searched second-order coefficient matches the true value, the final target integration results by the azimuth FFT and the subaperture FFT can be expressed as

$$\begin{aligned}sS'_{t,l}\left(t_r,f_m,f_l\right)&=LA''_t\text{sinc}\left[B\left(t_r-\frac{2R_0}{c}\right)\right]\\&\times\text{sinc}\left[T_c\left(f_m+\frac{2}{\lambda}v_e\right)\right]\\&\times\text{sinc}\left[N_c\left(f_l+\frac{2}{\lambda}v_eT_c\right)\right]\\&\times\exp\left[-j\frac{4\pi}{\lambda}\left(R_0-\frac{D}{2}\cos\theta_{\text{Azi},t}\sin\theta_{\text{El},t}\right)\right]\end{aligned} \tag{41}$$

where $A''_t=MP_{\text{av}}T_cBG_T(\theta_{\text{Azi},t},\theta_{\text{El},t})G_{R-\text{Sub}}(\theta_{\text{Azi},t},\theta_{\text{El},t})\lambda^2\sigma/(4\pi)^3R_0^4L_s$ is the target amplitude after implementing the spatial domain synthesis and subaperture coherent integration.

After that, the target energy has been finally integrated by the above steps, and thus the high threshold CFAR technique can be utilized to accomplish the final target detection, which can be denoted as

$$T_{\text{HighThre}}=sS'_{t,l}\left(t_r,f_{m,l}\right)\underset{H_0}{\overset{H_1}{\gtrless}}V_{\text{HT}} \tag{42}$$

where V_{HT} is the high detection threshold determined by the specified false alarm and detection probability [43]. The above process flows are repeated for each possible target point determined by (37). As a result, the false alarms can be effectively removed and the true moving targets can be well extracted.

V. SIMULATION RESULTS AND ANALYSIS

A. Point Target Simulation Results

This section focuses on the effectiveness of the proposed SAKTMF method, and the radar system parameters are given in Table I. A moving target with second-order motion model is used in the simulation, where the radial velocity and radial acceleration are set as 80 m/s and 20 m/s^2, respectively. The white Gaussian noise is added for evaluation of the proposed method in the case of noise, where the range-compressed SNR of this moving target is set as 5 dB.

TABLE II
AIR MOVING TARGET PARAMETERS

	Range cell	RCS	v_e	v_x
Tar 1	200	0.5 m^2	100 m/s	200 m/s
Tar 2	300	0.5 m^2	150 m/s	250 m/s
Tar 3	400	0.5 m^2	200 m/s	300 m/s

The processing results of each step in the proposed SAKTMF method are provided in Fig. 5. The range-compressed target profiles before and after liner RM correction are shown in Fig. 5(a) and (b), respectively. Clearly, RM of this target is greatly relieved by using the well-known KT. Subsequently, the whole-aperture return is divided into 60 subapertures and each subaperture contains 50 pulses. Preliminary integration is carried out by performing azimuth FFT, and the integration results of the subaperture 10, 20, and 40 are exhibited in Fig. 5(c)–(e), respectively. From these figures, it can be observed that the focused positions both in range and Doppler directions varies with different subapertures. To integrate entire target energy, phase compensation and subaperture coherent integration are implemented, as introduced in Section III-B. The accumulation values vary with the searching target second motion parameter is shown in Fig. 5(f), where the peak position corresponds to the target second motion parameter estimation. The compensated subaperture integration results with respect to the optimal acceleration estimation of subaperture 20 and 40 are shown in Fig. 5(g) and (h), respectively. It can be observed that peak position variation between subapertures is eliminated. After that, a secondary accumulation result at 132th range gate by the proposed SAKTMF is shown in Fig. 5(i), where a distinct peak is formed in the subaperture-frequency and azimuth-frequency domain.

In order to make a comparison with existing methods under low SNR environment, the GRFT method [16], HI method [38], and ACCF method [33] are added for the comparative methods. The SNR decreases to -20 dB, and the others simulation conditions keep the same as used in Fig. 5. The accumulation results of different methods are shown in Fig. 6, from which it can be observed that the ACCF method and HI method are invalid in this case since the performance loss is unacceptable in the low SNR environment. On the contrary, the proposed method still work well as the optimal GRFT does, in virtue of the entire coherent integration gain without extra SNR loss.

B. Air Moving Target Detection in an SBEWR System

In this section, the simulation processing results are provided to verify the proposed algorithm. The parameters of an L-band SBEWR system [20] and three AMTs in this simulation are listed in Tables II and III, respectively.

Due to the high-speed moving characteristics of the satellite platform, the clutter spectrum is significantly broadened, as shown in Fig. 7(a). Fig. 7(b) shows the clutter rejection results with respect to the whole-aperture data by directly applying the

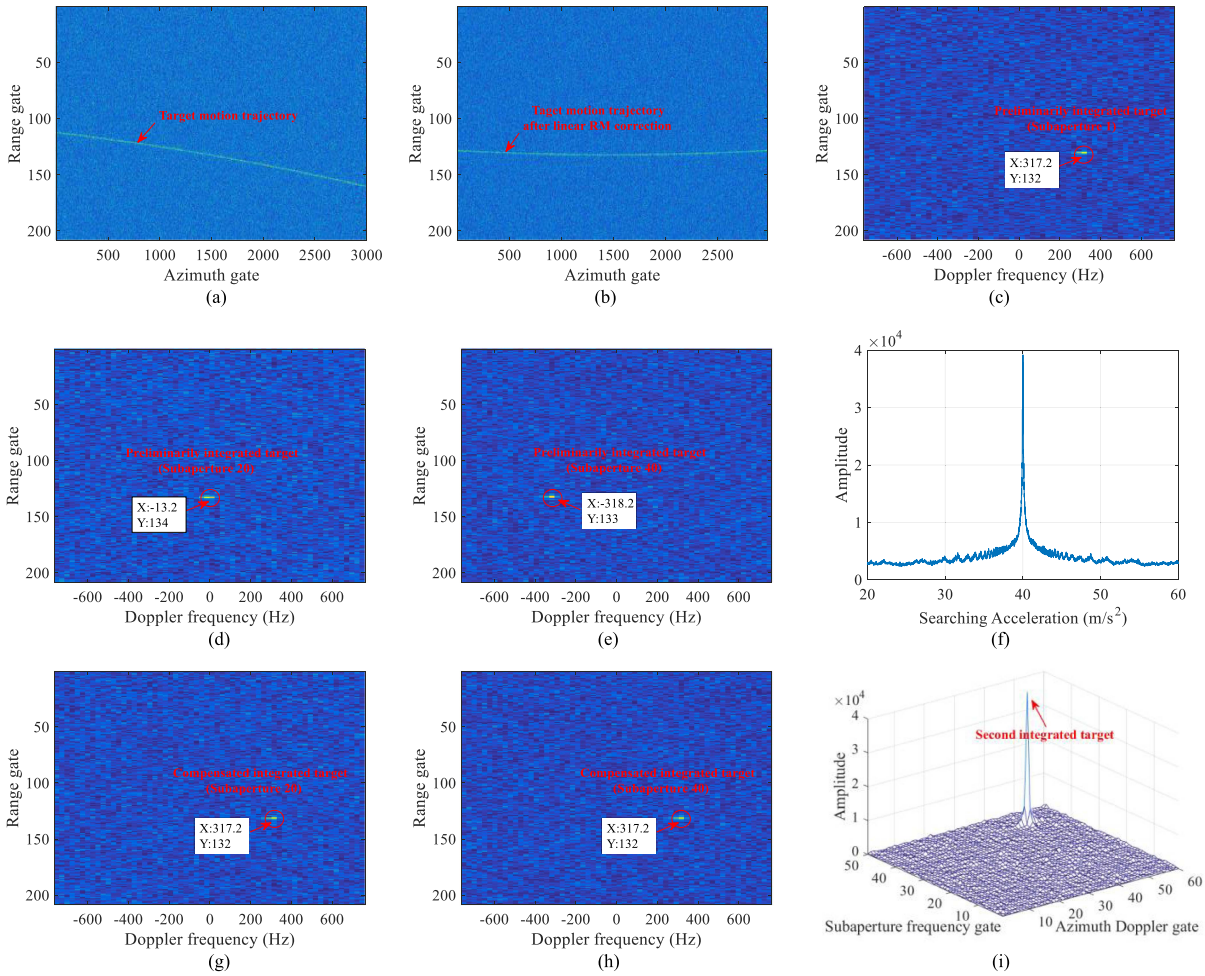

Fig. 5. Processing results for the proposed SAKTMF method. (a) Range profiles in the range-compression domain. (b) Range profiles after linear RM correction by KT. (c) Preliminarily integrated results for subaperture 10. (d) Preliminarily integrated results for subaperture 20. (e) Preliminarily integrated results for subaperture 40. (f) Accumulation value varies with searching acceleration. (g) Compensated integration results for subaperture 20. (h) Compensated integration results for subaperture 40. (i) Final integration results by proposed SAKTMF method in subaperture-frequency and azimuth-frequency domain.

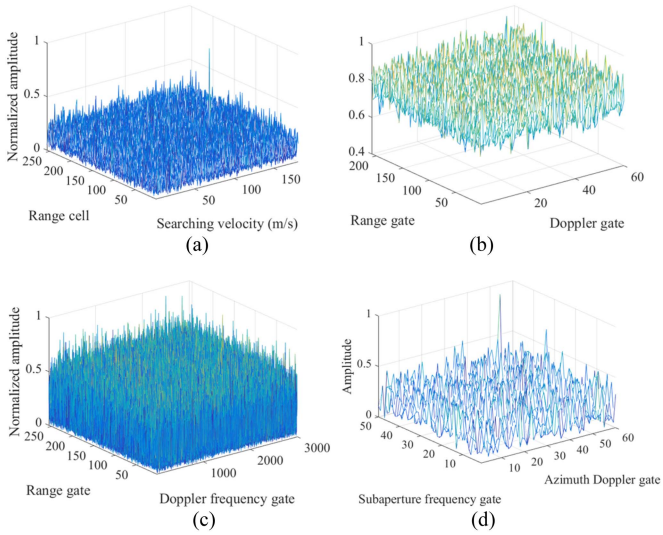

Fig. 6. Accumulation results by different methods under low SNR environment. (a) GRFT method. (b) HI method. (c) ACCF method. (d) Proposed SAKTMF method.

TABLE III
L-BAND SBEWR SYSTEM PARAMETERS

Parameter	Value	Parameter	Value
Average power	4 kW	Radar altitude	506 km
Center frequency	1.26 GHz	Radar speed	7609 m/s
LFM bandwidth	3 MHz	Noise factor	3 dB
Pulse repetition frequency	4000 Hz	System loss	6 dB
Coherent processing time	400 ms	Tx weighting gain	42.1 dB
Number of channels	32	Rx weighting gain	42.1 dB
Amplitude-phase error	0.5 dB/5 Deg	Antenna length	50 m
Orbit inclination	19 Deg	Antenna height	2 m
Clutter type	Hill	Elevation angle	60 Deg
Clutter model	Gamma	Azimuth angle	90 Deg

extended factor approach method [7]. Obviously, these uncooperative moving targets are significantly smeared along the range and Doppler directions and fail to be detected. The whole echo data are divided into eight temporal subapertures, and the range-Doppler spectrum with the first CFAR detection (8.5 dB) result of the reference subaperture after performing the KT and subaperture STAP is shown in Fig. 7(c), where Tar 1–Tar 3 are

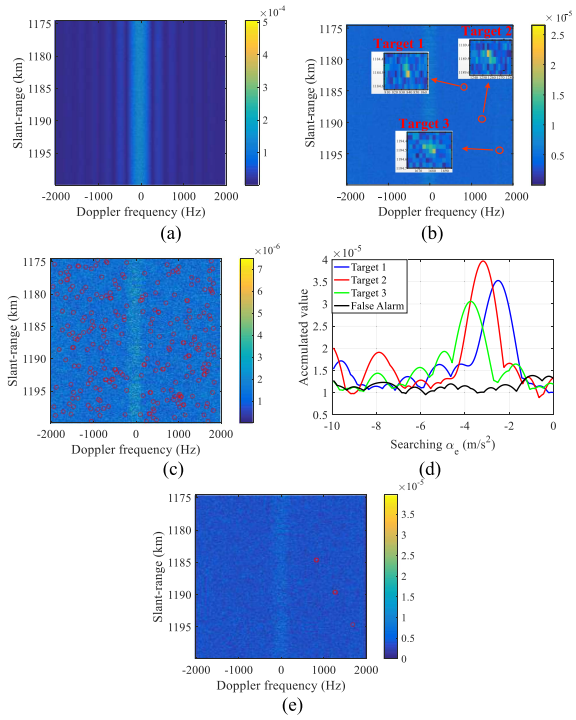

Fig. 7. Process results by the proposed SAKTMF method. (a) SBEWR echo spectrum before clutter suppression. (b) SBEWR echo spectrum after full aperture clutter suppression. (c) First CFAR detection (8.5 dB) results after subaperture clutter suppression. (d) Output amplitudes vary with searched $\hat{\alpha}_e$ for Tar 1–Tar 3. (e) High threshold (13.2 dB) CFAR detection results.

automatically detected with the red circle; in addition, some false alarms are also detected due to the low detection threshold. The final target output amplitudes varying with the searched α_e for Tar 1–Tar 3 and false alarm are depicted in Fig. 7(d), from which one can see that three peaks appear when the searched equivalent second coefficients match their true values. As for the false alarm point, no distinct peak is shaped, and thus they can be removed by subsequent high threshold CFAR detection according to (43). Finally, the second CFAR detection, with a detection threshold of 13.2 dB (false alarm rate 10^{-6}, detection probability 0.9), is performed with respect to the final focusing results, as displayed in Fig. 7(e), from which it can be seen that Tar 1–Tar 3 are effectively detected and the false alarms are effectively removed, indicating the effectiveness of the proposed SAKTMF method.

C. Detection Performance Analysis

In the following, a Monte Carlo simulation experiment is performed to validate the moving detection performance of the GRFT method, HI method [13], ACCF method [10], MTD method, and proposed SAKTMF method. The radar system parameters remain the same as those listed in Table I, the number of Monte Carlo simulations is 500, and the target equivalent radial velocity and acceleration are set as 200 m/s and 20 m/s^2, respectively. In addition, the temporal subaperture division status in the HI method and proposed SAKTMF method is consistent with those used in Fig. 5.

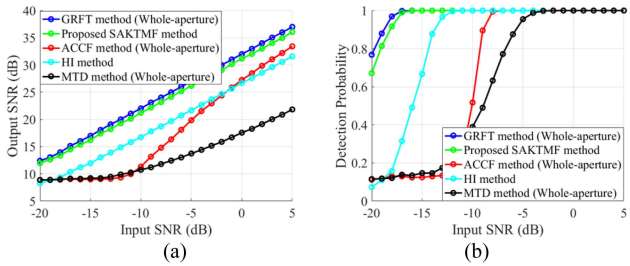

Fig. 8. Output SNR and detection probability curves against SNR. (a) Output SNR varies with input SNR. (b) Detection probability varies with input SNR.

As depicted in Fig. 8, the detection performance of the proposed SAKTMF method is very close to the optimal GRFT method and superior to the HI method in virtue of the coherent accumulation gain obtained from the different subapertures. The ACCF method suffers from SNR loss induced by nonlinear operation, and this loss becomes severe as the input SNR decreases. The MTD method without subaperture processing exhibits poor detection performance because of severe energy loss caused by DFM. Therefore, the proposed method can achieve a good balance between the computational complexity and target detection performance.

VI. Discussion

A. Algorithm Efficiency

The computational complexity of the proposed SAKTMF will be analyzed in this subsection, and some conventional algorithms, i.e., the GRFT method, HI method, and ACCF method are employed for comparisons in term of floating-point operations (Flops).

In this article, each time of the complex addition, complex multiplication, and real addition occupy computational complexity about 2 Flops, 6 Flops, and 1 Flops, respectively. As for N-point FFT, $5N\log_2 N$ Flops is required [39]. Assume that M_0 being parameter searching grids of each order. As established in Section III-B, the proposed SAKTMF method mainly contains four steps: KT, preliminary integration in each subaperture, phase compensation among subapertures, and subaperture FFT. As for KT, it can be implemented with a fast strategy [25], which contains four times of FFT and complex multiplication, resulting in computation complexity with $20N_rN_a\log_2 N_a + 24N_rN_a$ Flops. For the residual steps, the total parameters searching time is M_0^{K-2} and each searching process requires one-time complex multiplication for phase compensation, N_r time N_c-point FFT and N_c time N_r-point IFFT are consumed in preliminary integration process, and N_rN_a time L-point FFT for subaperture FFT. The computational complexities of the GRFT method, HI method, and ACCF-based method are summarized in Table IV for comparisons.

To clearly display the computational efficiency of above methods, a simulation is employed for comparisons based on Table IV, where azimuth sample number varies from 100 to 1000 and others values are set as follows: $N_r = 800$, $L = 4$, $M_0 = 5N_a$, and $K = 2$. From Fig. 9, it is clearly observed that the GRFT method suffers from the heavy computation

TABLE IV
COMPUTATIONAL COMPLEXITIES FOR DIFFERENT ALGORITHMS

Methods	Computational complexities (Flops)	Searching dimension
GRFT method	$8M_0^{K-1}N_rN_a$	*k–1* D dimension
HI method	$6LN_rN_c\log_2 N_c + M_0^{K-1}(L-1)$	*k–1* D dimension
ACCF-based method	$6(K-1)N_rN_a + 5N_rN_a\log_2 N_r + 5N_rN_a\log_2 N_a$	Without searching
Proposed SAKTMF method	$20N_rN_a\log_2 N_a + 24N_rN_a + M_0^{K-2}L(6N_rN_s + 5N_rN_s\log_2 N_r + 5N_rN_s\log_2 N_c + 5N_rN_s\log_2 L)$	*k–2* D dimension

TABLE V
OUTPUT SNRS FOR DIFFERENT METHODS

Methods	Output SNRs	Remarks
GRFT method	$SNR_{GRFT} = SNR_{In} + G_{Pc} + G_{GRFT}$	$G_{GRFT} = 10\log10(N_a)$
HI method	$SNR_{HI} = SNR_{In} + G_{Pc} + G_{HI}$	$G_{HI} = 10\log10(N_c) + 10\log10(\sqrt{L})$
ACCF-based method	$SNR_{ACCF} = SNR_{In} + G_{Pc} + G_{ACCF} - L_s$	$G_{ACCF} = 10\log10(N_a)$, $L_s \geq 3dB$
Proposed SAKTMF method	$SNR_{SAKTMF} = SNR_{In} + G_{Pc} + G_{SAKTMF} - L_0$	$G_{SAKTMF} = 10\log10(N_c) + 10\log10(L)$, $L_0 \in [0, 3dB]$

where SNR_{In} is the input SNR before pulse compression, $G_{Pc} = \sqrt{T_pB}$ denote the pulse compression gain, L_s and L_0 refer to energy loss induced by nonlinear operation and picket fence effect in FFT.

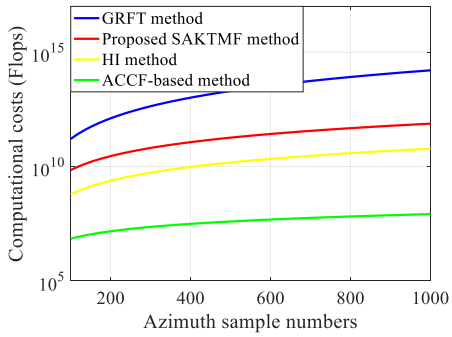

Fig. 9. Computational complexities comparisons for different methods.

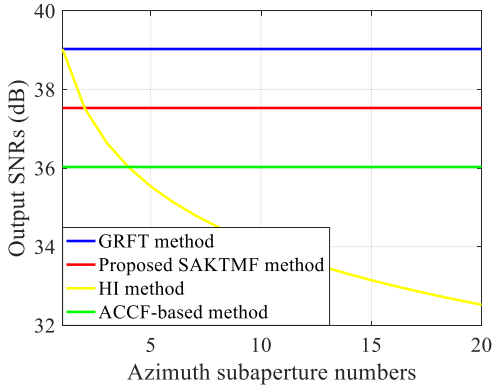

Fig. 10. Output SNRs varies with azimuth subaperture numbers for different methods (high input SNR environment).

costs because of the multidimension searching. In spite of the computation complexity is saved in the HI method and the ACCF method, performance degradation is acted as a cost. Compared with these methods, the computation complexity of the proposed SAKTMF is alleviated since searching dimension is reduced without sacrifice of detection performance loss.

B. Output SNR Analysis

In this subsection, the output SNR of the proposed method and existing methods are analyzed. Table V summarizes the relationship between the output SNRs and input SNR for different methods. Compared with the HI method [38], the integration gain of the proposed SAKTMF method is improved in virtue by the coherent integration gain among different subapertures.

In the next, another simulation is taken to demonstrate the theoretical output SNR performance varying with subaperture number based on Table V. Assume that a high SNR environment is established and a set of typical values are $L_s = 3$ dB, $SNR_{In} + G_{Pc} = 10$ dB, $N_a = 800$, $N_c = N_a/L$, $L_0 = 1.5$ dB, and subaperture number L varies from 1 to 20. According to the simulation results exhibited in Fig. 10, it can be seen that the output SNR of the traditional HI method is decreased as the subaperture number increase while others not. In addition, the output SNR of the proposed SAKTMF method is close to that of the optimal GRFT method thanks to the integration gains within and among subapertures.

C. Detection Threshold Settings

As for specified false alarm rate and detection probability, the corresponding detection threshold can be calculated by the following formula [44]:

$$V_T = 10\lg\left(\left(\sqrt{-\ln P_{f_a}} - \mathrm{erfc}^{-1}(2P_d)\right)^2 - 0.5\right)\ \mathrm{dB} \quad (43)$$

where P_{f_a} and P_d are the false alarm rate and detection probability, respectively, and $\mathrm{erfc}(\cdot)$ denotes the complementary error function.

According to (43), the high threshold V_{HT} can be calculated as 13.2 dB with $P_{f_a} = 10^{-6}$ and $P_d = 0.9$. As for the low threshold, it can be determined by $V_{\mathrm{LT}} = V_{\mathrm{HT}} - 10\log 10(L)$ to ensure extract the potential targets. However, the false alarm rate will be increased as the subaperture number increases in this case. To avoid this phenomenon, a minimum detection threshold (empirically, 8–9 dB) is set as the boundary value.

VII. Conclusion

In this article, a novel SAKTMF approach has been proposed to address target RM and DFM in a long observation time and improve detection performance for weak AMTs. The theoretical derivation and performance analysis of the proposed SAKTMF method are also provided. Based on the two steps coherent integration strategy, the proposed SAKTMF approach can achieve coherent integration both within subaperture and among subapertures during the long observation time with high computational efficiency.

In addition, the SAKTMF is applied in an SBEWR system with the AMT detection model to enhance target output SCNR by prolonging observation time, where the cuttler influence is taken into consideration. In this way, the potential hypothesis that the AMTs have been detected by using the conventional methods has been completely avoided. Benefiting from the above advantages, the SAKTMF method is very suitable to detect a high-speed and weak AMT as an alternative for SBEWR. Simulation results of different conditions also demonstrate the effectiveness of the proposed method.

Additional works on the statistical performance analysis and picket fence effect analysis of the proposed SAKTMF method and how to realize long-time coherent integration for maneuvering target by utilizing low-rank and sparse characteristics [45], [46], [47] will be under our future investigations.

References

[1] S. Pillai, B. Himed, and K. Y. Li, "Effect of earth's rotation and range foldover on space-based radar performance," *IEEE Trans. Aerosp. Electron. Syst.*, vol. 42, no. 3, pp. 917–932, Jul. 2006.

[2] G. Lavery, "Effect of antenna peak sidelobe levels on L-band space-based GMTI radar performance," in *Proc. IEEE Aerosp. Conf.*, 2005, pp. 2162–2169.

[3] J. Tian, W. Cui, and S. Wu, "A novel method for parameter estimation of space moving targets," *IEEE Geosci. Remote Sens. Lett.*, vol. 11, no. 2, pp. 389–393, Feb. 2014.

[4] J. B. Zheng, T. Su, H. W. Liu, G. S. Liao, Z. Liu, and Q. H. Liu, "Radar high-speed target detection based on the frequency-domain deramp-keystone transform," *IEEE J. Sel. Topics Appl. Earth Observ. Remote Sens.*, vol. 9, no. 1, pp. 285–294, Mar. 2015.

[5] J. B. Zheng, T. Su, W. T. Zhu, X. H. He, and Q. H. Liu, "Radar high-speed target detection based on the scaled inverse Fourier transform," *IEEE J. Sel. Topics Appl. Earth Observ. Remote Sens.*, vol. 8, no. 3, pp. 1108–1119, Mar. 2015.

[6] W. L. Melvin, "A STAP overview," *IEEE Trans. Aerosp. Electron. Syst.*, vol. 19, no. 1, pp. 13–35, Jan. 2004.

[7] R. Dipietro, "Extended factored space-time processing for airborne radar systems," in *Proc. 26th Asilomar Conf. Signals, Syst. Comput.*, Oct. 1992, pp. 425–430.

[8] L. E. Brennan, D. J. Piwinski, and F. M. Standaher, "Comparison of space-time adaptive processing approaches using experimental airborne radar data," in *Proc. IEEE Int. Radar Conf.*, 1993, pp. 176–181.

[9] H. Wang and L. Cai, "On adaptive spatial-temporal processing for airborne surveillance radar systems," *IEEE Trans. Aerosp. Electron. Syst.*, vol. 30, no. 3, pp. 660–670, Jul. 1994.

[10] M. Y. Zhan et al., "Performance analysis of space-borne early warning radar for AMTI," in *Proc. 6th Asia-Pacific Conf. Synthetic Aperture Radar*, 2019, pp. 1–6.

[11] X. Rao, H. Tao, J. Su, X. Guo, and J. Zhang, "Axis rotation MTD algorithm for weak target detection," *Digit. Signal Process.*, vol. 26, pp. 81–86, 2014.

[12] X. Fang, R. Min, Z. Cao, and Y. Pi, "High-order RM and DFM correction method for long-time coherent integration of highly maneuvering target," *Signal Process.*, vol. 162, pp. 221–233, Sep. 2019.

[13] B. D. Carlson, E. D. Evans, and S. L. Wilson, "Search radar detection and track with the Hough transform, part I: System concept," *IEEE Trans. Aerosp. Electron. Syst.*, vol. 30, no. 1, pp. 102–108, Jan. 1994.

[14] B. D. Carlson, E. D. Evans, and S. L. Wilson, "Search radar detection and track with the Hough transform. II. Detection statistics," *IEEE Trans. Aerosp. Electron. Syst.*, vol. 30, no. 1, pp. 109–115, Jan. 1994.

[15] J. Xu, J. Yu, Y. N. Peng, and X.-G. Xia, "Radon-Fourier transform for radar target detection, I: Generalized Doppler filter bank," *IEEE Trans. Aerosp. Electron. Syst.*, vol. 47, no. 2, pp. 1186–1202, Apr. 2011.

[16] J. Xu, X.-G. Xia, S.-B. Peng, J. Yu, Y.-N. Peng, and L.-C. Qian, "Radar maneuvering target motion estimation based on generalized Radon-Fourier transform," *IEEE Trans. Signal Process.*, vol. 60, no. 12, pp. 6190–6201, Dec. 2012.

[17] X. L. Chen, J. Guan, N. B. Liu, and Y. He, "Maneuvering target detection via Radon-fractional Fourier transform-based long-time coherent integration," *IEEE Trans. Signal Process.*, vol. 62, no. 4, pp. 939–953, Feb. 2014.

[18] X. L. Li, G. L. Cui, W. Yi, and L. J. Kong, "Coherent integration for maneuvering target detection based on Radon-Lv's distribution," *IEEE Signal Process. Lett.*, vol. 22, no. 9, pp. 1467–1471, Sep. 2015.

[19] X. L. Li, Z. Sun, T. Zhang, W. Yi, G. L. Cui, and L. J. Kong, "WRFRFT-based coherent detection and parameter estimation of radar moving target with unknown entry/departure time," *Signal Process.*, vol. 166, Jul. 2019, Art. no. 107228.

[20] L. Lin, G. Sun, Z. Cheng, and Z. He, "Long-time coherent integration for maneuvering target detection based on ITRT-MRFT," *IEEE Sensors J.*, vol. 20, no. 7, pp. 3718–3731, Apr. 2020.

[21] D. Pastina et al., "Maritime moving target long time integration for GNSS-based passive bistatic radar," *IEEE Trans. Aerosp. Electron. Syst.*, vol. 54, no. 6, pp. 3060–3083, Dec. 2018.

[22] K. Jin, G. Li, T. Lai, T. Jin, and Y. Zhao, "A novel long-time coherent integration algorithm for Doppler-ambiguous radar maneuvering target detection," *IEEE Sensors J.*, vol. 20, no. 16, pp. 9394–9407, Aug. 2020.

[23] X. L. Chen, J. Guan, N. B. Liu, W. Zhou, and Y. He, "Detection of a low observable sea-surface target with micromotion via the Radon-linear canonical transform," *IEEE Geosci. Remote Sens. Lett.*, vol. 11, no. 7, pp. 1225–1229, Jul. 2014.

[24] X. L. Chen, Y. Huang, N. B. Liu, J. Guan, and Y. He, "Radon-fractional ambiguity function-based detection method of low-observable maneuvering target," *IEEE Trans. Aerosp. Electron. Syst.*, vol. 51, no. 2, pp. 815–833, Apr. 2015.

[25] D. Zhu, Y. Li, and Z. Zhu, "A keystone transform without interpolation for SAR ground moving-target imaging," *IEEE Geosci. Remote Sens. Lett.*, vol. 4, no. 1, pp. 18–22, Jan. 2007.

[26] J. Tian, W. Cui, X.-G. Xia, and S. L. Wu, "Parameter estimation of ground moving targets based on SKT-DLVT processing," *IEEE Trans. Comput. Imag.*, vol. 2, no. 1, pp. 13–26, Mar. 2016.

[27] L. Kong, X. Li, G. Cui, W. Yi, and Y. Yang, "Coherent integration algorithm for a maneuvering target with high-order range migration," *IEEE Trans. Signal Process.*, vol. 63, no. 17, pp. 4474–4486, Sep. 2015.

[28] G. Li, X.-G. Xia, and Y. N. Peng, "Doppler keystone transform: An approach suitable for parallel implementation of SAR moving target imaging," *IEEE Geosci. Remote Sens. Lett.*, vol. 5, no. 4, pp. 573–577, Oct. 2008.

[29] C. L. Wang, B. Jiu, and H. W. Liu, "Maneuvering target detection in random pulse repetition interval radar via resampling-keystone transform," *Signal Process.*, vol. 181, Apr. 2021, Art. no. 107899.

[30] P. H. Huang, G. S. Liao, Y. Zhiwei, X.-G. Xia, J.-T. Ma, and J. T. Ma, "Long-time coherent integration for weak maneuvering target detection and high-order motion parameter estimation based on Keystone transform," *IEEE Trans. Signal Process.*, vol. 64, no. 15, pp. 4013–4026, Aug. 2016.

[31] S. Q. Zhu, G. S. Liao, D. Yang, and H. H. Tao, "A new method for radar high-speed maneuvering weak target detection and imaging," *IEEE Geosci. Remote Sens. Lett.*, vol. 11, no. 7, pp. 1175–1179, Jul. 2014.

[32] Y. L. Neo, F. Wong, and I. G. Cumming, "A two-dimensional spectrum for bistatic SAR processing using series reversion," *IEEE Geosci. Remote Sens. Lett.*, vol. 4, no. 1, pp. 93–96, Jan. 2007.

[33] X. L. Li, G. L. Cui, W. Yi, and L. J. Kong, "A fast maneuvering target motion parameters estimation algorithm based on ACCF," *IEEE Signal Process. Lett.*, vol. 22, no. 3, pp. 270–274, Mar. 2015.
[34] X. L. Li, G. L. Cui, W. Yi, and L. J. Kong, "Fast coherent integration for maneuvering target with high-order range migration via TRT-SKT-LVD," *IEEE Trans. Aerosp. Electron. Syst.*, vol. 52, no. 6, pp. 2803–2814, Dec. 2016.
[35] J. Tian, W. Cui, X.-G. Xia, and S. L. Wu, "Parameter estimation of ground moving targets based on SKT-DLVT processing," *IEEE Trans. Comput. Imag.*, vol. 2, no. 1, pp. 13–26, Mar. 2016.
[36] X. L. Li, G. L. Cui, W. Yi, and L. J. Kong, "Sequence-reversing transform-based coherent integration for high-speed target detection," *IEEE Trans. Aerosp. Electron. Syst.*, vol. 53, no. 3, pp. 1573–1580, Jun. 2017.
[37] P. H. Huang, G. Liao, Z. Yang, X.-G. Xia, J.-T. Ma, and X. Zhang, "A fast SAR imaging method for ground moving target using a second-order WVD transform," *IEEE Trans. Geosci. Remote Sens.*, vol. 54, no. 4, pp. 1940–1956, Apr. 2016.
[38] W. Yi, H. Jiang, T. Kirubarajan, L. Kong, and X. Yang, "Track-before-detect strategies for radar detection in G0-distributed clutter," *IEEE Trans. Aerosp. Electron. Syst.*, vol. 53, no. 5, pp. 2516–2533, Oct. 2017.
[39] Y. Barniv and O. Kella, "Dynamic programming solution for detecting dim moving targets part II: Analysis," *IEEE Trans. Aerosp. Electron. Syst.*, vol. AES-23, no. 6, pp. 776–788, Nov. 1987.
[40] Z. He, Y. Yang, and W. Chen, "A hybrid integration method for moving target detection with GNSS-based passive radar," *IEEE J. Sel. Topics Appl. Earth Observ. Remote Sens.*, vol. 14, no. 10, pp. 1184–1193, Nov. 2020.
[41] L. Zhao, H. Tao, W. Chen, and D. Song, "Maneuvering target detection based on subspace subaperture joint coherent integration," *Remote Sens.*, vol. 13, no. 10, pp. 1948–1967, May 2021.
[42] H. Chen, X. Li, W. Yi, X. Fang, and L. lei, "Coherent integration algorithm for high-speed maneuvering targets based on RFT and segmented processing," *J. Signal Process.*, vol. 37, no. 7, pp. 1189–1197, Jul. 2021.
[43] X. L. Li, Y. Yang, Z. Sun, G. Cui, and T. S. Yeo, "Multi-frame integration method for radar detection of weak moving target," *IEEE Trans. Veh. Technol.*, vol. 70, no. 4, pp. 3609–3624, Apr. 2021.
[44] B. R. Mahafza and A. Z. Elsherbeni, *MATLAB Simulations for Radar Systems Design*. London, U.K.: Chapman & Hall, 2003.
[45] G. Xu, B. J. Zhang, J. L. Chen, and W. Hong, "Structured low-rank and sparse method for ISAR imaging with 2D compressive sampling," *IEEE Trans. Geosci. Remote Sens.*, vol. 60, no. 10, pp. 2–40, Nov. 2022.
[46] G. Xu, B. J. Zhang, H. W. Yu, J. L. Chen, M. D. Xing, and W. Hong, "Sparse synthetic aperture radar imaging from compressed sensing and machine learning: Theories, applications and trends," *IEEE Geosci. Remote Sens. Mag.*, vol. 10, no. 4, pp. 32–69, Dec. 2022.
[47] L. Chen, X. Jiang, Z. Li, X. Z. Liu, and Z. X. Zhou. "Feature-enhanced speckle reduction via low-rank and space-angle continuity for circular SAR target recognition," *IEEE Trans. Geosci. Remote Sens.*, vol. 58, no. 11, pp. 7734–7752, Nov. 2020.

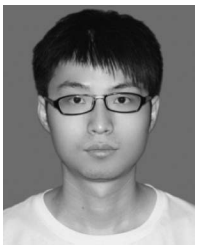

Muyang Zhan was born in Hubei, China. He received the B.S. degree in electronic information engineering from the Huanggang Normal University, Hubei, China, in 2015, the M.S. degree in electronics and communications engineering from the Chongqing University, Chongqing, China, in 2018, and the Ph.D. degree in information and communication engineering from the Shanghai Jiao Tong University, Shanghai, China, in 2022.

Since July 2022, he has been an Algorithm Engineer for Radar Systems with the Shanghai Aerospace Electronic Technology Institute, Shanghai, China. His research interests include ISAR imaging, parameter estimation, and spaceborne radar system design.

Chanjuan Zhao was born in Hubei, China. She received the B.S. degree in communication engineering from the Xidian University, Xi'an, China, in 2004, and the M.S. degree in signal and information processing from the Shanghai Aerospace Electronic Technology Institute, Shanghai, China, in 2007. She is currently working toward the Ph.D. degree in electrical engineering with the Xidian University.

Since 2007, she has been a Radar System Engineer with the Shanghai Aerospace Electronic Technology Institute. Her research interests include tracking-and-guiding radar and radar system design.

Kun Qin was born in Jiangsu, China. He received the B.S. degree in communication engineering from the Nanjing University of Technology, Xi'an, China, in 2004, and the M.S. degree in signal and information processing from the Shanghai Aerospace Electronic Technology Institute, Shanghai, China, in 2007. He is currently working toward the Ph.D. degree in electrical engineering with the Xidian University, Xi'an, China.

Since 2007, he has been a Radar System Engineer with the Shanghai Aerospace Electronic Technology Institute. His research interests include tracking-and-guiding radar and radar system design.

Penghui Huang (Member, IEEE) was born in Jiangxi, China. He received the B.S. and Ph.D. degrees in electrical engineering from the Xidian University, Xi'an, China, in 2012 and 2017, respectively.

He joined the School of Electronic Information and Electrical Engineering, Shanghai Jiao Tong University, Shanghai, China, in 2017. He was an Assistant Professor, from 2017 to 2021, and he is currently an Associate Professor and a Ph.D. Adviser. His research interests include spaceborne early warning radar system design, space–time adaptive processing, multichannel sea clutter modeling, simulation, space–time property analysis, and robust suppression, distributed spaceborne wide-area surveillance radar signal processing with ground moving target indication and air moving target indication, spaceborne HRWS–SAR imaging, ISAR imaging, and weak target detection and tracking.

Dr. Huang was the recipient of the Prize for Excellent Ph.D. degree dissertation of the Chinese Institute of Electronics education in 2017, and also the recipient of the Prize for Excellent Ph.D. degree dissertation of the Shaanxi Province in 2019. He is a Reviewer of the IEEE TRANSACTIONS ON GEOSCIENCE AND REMOTE SENSING, the IEEE TRANSACTIONS ON AEROSPACE AND ELECTRONIC SYSTEMS, the IEEE TRANSACTIONS ON SIGNAL PROCESSING, the IEEE JOURNAL OF SELECTED TOPICS IN APPLIED EARTH OBSERVATIONS AND REMOTE SENSING, the IEEE SENSOR JOURNALS, the IEEE GEOSCIENCE AND REMOTE SENSING LETTERS, etc.

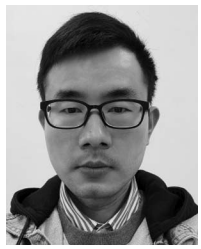

Ming Fang was born in Zhejiang, China. He received the B.S. degree in intelligent science and technology and the Ph.D. degree in signal and information processing from the Xidian University, Xi'an, China, in 2010 and 2016, respectively.

Since October 2016, he has been an Algorithm Engineer for Radar Systems with the Shanghai Aerospace Electronic Technology Institute, Shanghai, China. His research interests include waveform design and radar system design.

Chunlei Zhao was born in Suihua, Heilongjiang, China. He received the B.S. degree in electronic and information engineering, and the M.S. and Ph.D. degrees in information and communication engineering from the Harbin Institute of Technology, Harbin, China, in 2013, 2015, and 2020, respectively.

Since November 2020, he has been an Algorithm Engineer for Radar Systems with the Shanghai Aerospace Electronic Technology Institute. His research interests include array signal processing, parameter estimation, compressive sensing, and optimization.